Food Chemistry: X 27 (2025) 102414

Contents lists available at ScienceDirect

Food Chemistry: X

journal homepage: www.sciencedirect.com/journal/food-chemistry-x

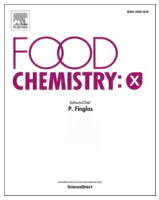

Preparation of polysaccharide-based films synergistically reinforced by tea polyphenols and graphene oxide

Zixuan Li [a], Mohammad Rizwan Khan [b], Naushad Ahmad [b], Wanli Zhang [a,*], Gulden Goksen [c,*]

[a] School of Food Science and Engineering, Hainan University, Haikou 570228, PR China
[b] Department of Chemistry, College of Science, King Saud University, Riyadh 11451, Saudi Arabia
[c] Department of Food Technology, Vocational School of Technical Sciences at Mersin Tarsus Organized Industrial Zone, Tarsus University, 33100, Mersin, Turkey

ARTICLE INFO

Keywords:
Film properties
Pectin films
Preservation applications

ABSTRACT

In this study, pectin (PE) composite films containing tea polyphenol (TP) and graphene oxide (GO) were developed. The effects of TP and GO on the appearance, structure, mechanical properties, barrier properties, hydrophobicity, and antioxidant properties of pure PE films were investigated. The results demonstrated that the addition of 1 % *w*/w TP and 1 % w/w GO increased the tensile strength (TS) and elongation at break (EB) of the composite films to 20.22 MPa and 34.18 %, respectively. Additionally, the water vapor permeability (WVP) was reduced to 0.67 ± 0.17 ($\times 10^{-10}$ $g^{-1}s^{-1}Pa^{-1}$), and both the moisture content and water contact angle were significantly decreased. Furthermore, the incorporation of TP enhanced the antioxidant properties of the composite films and demonstrated the slow-release capability of TP. Blueberry fruits packaged in PE-TP-GO film maintained an optimal appearance after eight days of storage at 25 °C, with a reduction in shrinkage index of approximately 29.4 % compared to those packaged in the PE film.

1. Introduction

The consumption of petroleum-based packaging materials has been substantial in recent decades. However, increasing awareness of safety and environmental concerns linked to their usage has prompted a quest to develop novel, biodegradable natural biopolymer materials (Zhang, Zhang, Cao, & Jiang, 2021). Pectin (PE) is a cell wall polysaccharide from plants, predominantly composed of galacturonic acid, which comprises approximately 70 % of its structure (Mohnen, 2008). PE serves as a frequently employed film-forming polysaccharide owing to its gelation, degradability, biocompatibility, and excellent water solubility (Gao, He, Sun, He, & Zeng, 2019). Numerous studies have explored the use of PE in food packaging films and edible coatings. For instance, incorporating plant extracts like fennel essential oil and potato peel extract into nano chitosan and PE-based films has enhanced the antimicrobial and antioxidant properties of the packaging (Sadadekar et al., 2023). Additionally, incorporating inorganic non-metallic materials, such as Zeolite Y and graphene oxide (GO), has improved the mechanical and barrier properties of the films (Nesic, Meseldzija, Cabrera-Barjas, & Onjia, 2022). Therefore, the addition of other material enhancers to address the challenges related to processing and mechanical properties of single-pectin materials may expand the application prospects of this biopolymer.

Tea polyphenols (TP) stand out as the primary potent chemical constituents in tea (Senanayake, 2013). With favorable attributes such as good water solubility, high antioxidant activity, biocompatibility, and low viscosity, TP can be incorporated into various polymers, including polysaccharides, polyvinyl alcohols, and proteins (Yang et al., 2021). Leveraging TP as an active ingredient in materials has facilitated the development of a spectrum of biodegradable packaging options imbued with antioxidant properties (Chen & Chi, 2021). Yang et al. (2024) prepared water-insoluble tea polyphenol nanoparticles (WI-TPN) to activate the PE film. WI-TPN has good compatibility with the film, which can improve the mechanical properties of the film as a filler and also give the film unique biological activity. In addition, enhancing the release properties of TP in biopolymer-based packaging films is crucial for improving the effectiveness of food packaging films.

Graphene is a two-dimensional material composed of a single layer of carbon atoms arranged in a hexagonal honeycomb pattern. Given its distinctive material attributes, graphene has emerged as a focal point of research in various realms of materials science in recent years (Yoo, Shin, Yoon, & Park, 2014). GO is rich in reactive oxygen-containing

* Corresponding authors.
E-mail addresses: mrkhan@ksu.edu.sa (M.R. Khan), anaushad@ksu.edu.sa (N. Ahmad), zwl@hainanu.edu.cn (W. Zhang), guldengoksen@tarsus.edu.tr (G. Goksen).

https://doi.org/10.1016/j.fochx.2025.102414
Received 26 December 2024; Received in revised form 20 March 2025; Accepted 24 March 2025
Available online 26 March 2025

functional groups, including the presence of hydroxyl, ketone and epoxy groups, and has high hydrophilicity, good biocompatibility and high specific surface area (2600 m^2 g^{-1}) (Guo, Duan, Cui, & Zhu, 2015; Lee et al., 2010). Many studies have confirmed that the incorporation of GO significantly enhances the mechanical and barrier properties of materials. For instance, chitosan/cerium oxide/GO films exhibit superior barrier and mechanical properties compared to other films (Panda, Dash, Yang, & Chang, 2022). In addition, a sodium alginate-gelatin-GO ternary composite film with 0.5 % GO addition demonstrated the best strength and ductility in a study by Yang et al. (2020). In other studies, such as poly (vinyl alcohol) composite films (Liu et al., 2016) and chitosan composite films (Zuo et al., 2013), the addition of GO has also resulted in films with excellent biocompatibility and mechanical properties. Therefore, GO serves as an effective reinforcing filler in the preparation of biocompatible composites and has significant potential for various applications. Additionally, studies have shown that GO, as a cross-linking agent, can synergistically enhance the performance of biopolymer-based films containing phenolic substances and improve the release characteristics of these phenolic compounds (Zhang, Cao, & Jiang, 2022; Zhang, Li, & Jiang, 2020).In summary, GO and TP can function as cross-linkers, enhancing the properties of biopolymer-based food packaging films such as PE. However, no study to date has examined the impact of the combined addition of GO and TP on the properties of biopolymer-based food packaging films. It is therefore hypothesized that GO and TP may synergistically improve the overall properties of PE films, with GO potentially enhancing the release characteristics of TP.

In this study, a PE-TP-GO composite system was investigated using the solution casting method. Pectin was used as the matrix polymer, TP as the antioxidant component, and GO was incorporated to enhance the mechanical and barrier properties of the pure pectin film. The primary objectives were to improve the comprehensive performance of the composite membrane and optimize the release characteristics of TP. The microstructure of the PE-TP-GO composite blended films was further analyzed using scanning electron microscopy (SEM), Fourier transform infrared spectroscopy (FTIR), and thermogravimetric analysis (TGA) and the physical and chemical properties, such as antioxidant performance and barrier capacity, were determined. The effectiveness of the composite film in preserving blueberry fruits was then assessed by monitoring quality changes throughout the storage period, including the total preservation time, to validate the composite film's capability to extend food freshness.

2. Materials and methods

2.1. Materials

PE was obtained from Shanghai McLean Biochemical Technology Co., LTD. (galacturonic acid ≥74.0 %, degree of methyl esterification >50), tea polyphenol (AR, concentration 98 %) was obtained from Shanghai Yuanye Biotechnology Co., LTD., glycerol (MW: 92.09 g/mol) were sourced from Shanghai Shenggong Biochemical Engineering Co., LTD and GO (2 mg/mL) aqueous solution was procured from Tanfeng Tech. Inc. ABTS (2,2′-azinobis(3-ethylbenzothiazoline-6-sulfonic acid) diammonium salt, purity ≥98 %) and DPPH (1,1-diphenyl-2-picrylhydrazyl radical, purity ≥98 %) were purchased from Aladdin Biochemical Technology Co. Blueberries were purchased from a local market in Hainan, selecting fruits of uniform size, fullness, and smoothness for the preservation experiment. All other reagents utilized were of analytical purity.

2.2. Preparation of films

The films were fabricated via a casting process according to the previous literature (Zhang & Jiang, 2020). Initially, 2 g of PE powder was fully dissolved in 100 mL 75 °C distilled water, and the mixture was stirred at 75 °C and 800 rpm by magnetic stirring for 2 h until complete dissolution, yielding a 2 % (*w/v*) PE base solution. Then add 30 % (*w*/w) glycerin for plasticizing, and stir for half an hour to make the plasticizer distribution uniform. Subsequently, 204.08 mg TP was dissolved in 10 mL of distilled water to produce a 1 % (w/w) TP solution. Similarly, add 1 % (w/w) GO solution into the PE base solution. Following this, film-forming solutions of PE-TP and PE-GO were formulated by introducing 1 % (w/w) TP solution and 1 % (w/w) GO aqueous solution, respectively, into the PE base solution. Additionally, a PE-TP-GO film-forming solution was prepared by the simultaneous addition of 1 % (w/w) TP solution and 1 % (w/w) GO aqueous solution to the PE base solution. Homogenization of all prepared film-forming solutions was achieved using a homogenizer at 7000 rpm for 5 min, followed by sonication for 30 min to remove air bubbles. The PE, PE-TP, PE-GO, and PE-TP-GO film forming solution, each comprising 20 mL, were poured into 9 cm-diameter polystyrene petri dishes and subsequently dried in an oven maintained at 50–60 °C. After 24 h, the films were meticulously removed from the polystyrene petri dishes and allowed to equilibrate for 48 h in a desiccator at 25 °C and 60 % relative humidity.

2.3. Characterizations of composite films

2.3.1. FTIR analysis

The FTIR measurements of distinct groups of PE film samples were primarily referenced from our earlier investigation (Yang et al., 2023). Specifically, a Fourier infrared spectrometer (Thermo Scientific Nicolet iS5, Grafo Industrial Equipment (Suzhou) Co. Ltd., Waltham, MA, USA) was employed to scan the film samples 32 times with a resolution of 4 cm^{-1} within the wavenumber range of 4000–400 cm^{-1}.

2.3.2. XRD analysis

The crystallinity of the film samples was measured through X-ray diffraction, utilizing an X-ray diffractometer (Rigaku SmartLab, Japan Institute of Technology, Chiba, Japan) for characterization. The scanning range spanned from 20° - 80° and the scanning rate is 2°/min.

2.3.3. TGA analysis

A TGA (DTG-60 Shim ADZU, Japan) was used to evaluate the thermal stability of film samples. This analysis was conducted under a flowing inert gas (nitrogen) environment, with a heating rate of 10 °C/min across a temperature range from 30 to 800 °C.

2.3.4. Microscopic morphology by SEM

A scanning electron microscope (Hitachi SU8010) was used to examine the microscopic morphology of film samples. The film sample (0.5 × 0.5 cm^2) was fixed on the copper net and observed after gold spraying. The film samples were freeze-fractured in liquid nitrogen to observe the cross-section. The surface of the film was observed at 1000×, with a voltage set to 2.0 kV, and the cross-section was observed at 2000×, with a voltage set to 3.0 kV.

2.4. Physical and mechanical properties

2.4.1. Mechanical properties

A texture tester (TA-XT plus 40,762, Stable Micro Systems, Inc., Godalming, UK) was employed to test the mechanical properties of the film samples. Initially, the film samples were trimmed to dimensions of 10 mm × 50 mm. The thickness of the rectangular strips was measured by employing a digital micrometer with an accuracy of 0.001 mm. Subsequently, the initial tensile length of the texture analyzer was established at 30 mm, with a tensile rate set at 1 mm/s. Tensile tests were conducted on the samples to ascertain their tensile strength (TS) and elongation at break (EB). Following the rupture of the film sample under tension, the instrument's tensile probe automatically reverted to its initial position. The TS and EB of the films were then calculated d using the subsequent formulas. Each film was measured at least five times. Three repetitions of every kind of sample were conducted.

$$\text{Tensile strength (MPa)} = \frac{F}{x \times w}$$

$$\text{Elongation at break (\%)} = \frac{\Delta x}{x_0} \times 100$$

Where F represents the film breaking stress (N), x denotes the film thickness (mm), w indicates the film width (mm), and Δx and x_0 respectively represent the extension distance (mm) and the initial length of the film.

2.4.2. Color and opacity

The color parameters L^* (brightness), a^* (green to red), and b^* (yellow to blue) of the films were determined employing a colorimeter (Model NF333, Nippon Denshoku Industries, Tokyo, Japan). Ten repetitions of every kind of sample were conducted.

The opacity of the samples was assessed following previously reported methods (Miao, Zhang, & Lu, 2021). Initially, the sample films were cut into rectangular strips. Subsequently, the absorbance of the film samples was measured over the 200–800 nm wavelength range utilizing a UV spectrophotometer (UV-5500PC, Shanghai Yuan Analytical Co., Ltd., China). Ten repetitions of every kind of sample were conducted. The opacity was then determined using the following equation:

$$p = \frac{-log\,(T)}{m}$$

Where T represents the transmittance (%) of the film at 600 nm, and m signifies the thickness of the film (mm).

2.4.3. Moisture content (MC)

The direct drying method was employed to assess the MC. Three film samples of 10 mm × 50 mm were taken from each group, and their initial weights were recorded. Subsequently, these samples were dried to a constant weight at 110 °C, and their final weights were recorded post-drying. The MC was then determined using the equation given below.

$$\text{Moisture contents (\%)} = \frac{(\text{initial mass} - \text{final dry mass})}{\text{initial mass}} \times 100$$

2.4.4. Water vapor permeability (WVP) and water contact angle (WCA)

The WVP of the samples was measured using the weight gain method, adapted from Zhang et al. (2020) with some enhancements. Initially, anhydrous calcium chloride (5 g) was measured in a 50 mL conical flask. Film samples of different components were then covered on the flask opening and sealed with a fixed wrapping using a sealing film. Subsequently, the conical flask was placed in a chamber maintained at 25 °C and 60 % relative humidity. The flasks were weighed every 2 h for 2 consecutive days. The WVP was determined using the equation provided below.

$$\text{WVP} = \frac{\Delta m \times l}{\Delta p \times t \times e}$$

Where Δm is the weight change (g) and l is the thickness of the films (m). Δp, t and e denote the difference of permeation area vapor pressure (Pa), the interval time (s) and the penetration area of the film sample (m^2), respectively.

The WCA of the film was measured using an interfacial tension apparatus (OSA100C, Ningbo New Boundary Scientific Instrument Co., Ningbo, China). Specifically, the film sample (5 cm × 10 cm) was placed on the horizontal moving platform of the interface tension apparatus. A 10 μL water drop was then dropped onto the surface of the film using a microsyringe and WCA was immediately measured from both sides of the drop. WCA was measured at five random points in the film sample and average values are reported.

2.5. Antioxidant activity and slow-release property

2.5.1. Antioxidant activity

The antioxidant properties of film samples were assessed following a previously established method with minor modifications (Yang et al., 2023). Specifically, film samples (100 mg) were immersed in distilled water (10 mL) for 24 h to determine their DPPH radical scavenging capacity. After centrifugation at 10,000 rpm for 10 min at 4 °C, 1 mL of supernatant was combined with 3 mL of 1 mM DPPH solution (2,2-diphenyl-1-trinitrophenylhydrazine). The mixture was then incubated at room temperature in darkness for 30 min, and the absorption was measured at 517 nm. The result of DPPH free radical scavenging was calculated according to the formula:

$$\text{DPPH radical scavenging activity (\%)} = \frac{Abs_{DPPH} - Abs_{extract1}}{Abs_{DPPH}} \times 100$$

Where Abs_{DPPH} is the absorbance value of DPPH at 517 nm and $Abs_{extract1}$ is the absorbance value of the sample extract at 517 nm.

Similarly, the ABTS radical scavenging capacity of PE film samples was assessed as follows: A solution of 7 mM ABTS and 2.45 mM potassium persulfate was mixed in a 1:1 ratio and allowed to react under light-protected conditions for 16 h. The resulting solution was diluted until the absorbance reached approximately 0.80 ± 0.02 at 734 nm. For the assay, 0.1 mL of the supernatant from the film sample and 0.8 mL of the ABTS reagent were mixed and incubated for 10 min at room temperature in the dark. The absorption was then measured at 734 nm. The result of ABTS free radical scavenging was determined using the formula:

$$\text{ABTS radical scavenging activity (\%)} = \frac{Abs_{\text{ABTS}} - Abs_{extract2}}{Abs_{\text{ABTS}}} \times 100$$

Where Abs_{ABTS} is the absorbance value of DPPH at 734 nm and $Abs_{extract2}$ is the absorbance value of the sample extract at 734 nm.

2.5.2. Slow-release property

The TP release assay was conducted in 0.9 % saline with a minor adaptation following previously reported methods (Miao et al., 2021). The films were cut into 0.4 g pieces and immersed in 50 mL of 0.9 % saline solution. At intervals of 6 h, 12 h, 24 h, 2 days and 4 days, 4 mL of the released solution was sampled and replaced with an equal volume of saline. The collected sample solutions were analyzed for absorbance at 725 nm using the Folin-Ciocalteu method, and the results were quantified in terms of gallic acid equivalents using a gallic acid standard curve.

2.6. Application of PE composite films in blueberry fruits

Blueberry fruits were arranged at the base of a polyethylene plate dish. Each plate contained seven uniformly sized blueberry fruits. The tops of the plates were sealed with different components of film samples and the plates were stored at 25 °C, 70 % RH for 8 days. Changes in the appearance and weight loss of the blueberry fruits were monitored throughout the storage period. The fruit shrinkage index was calculated based on a previous study by He et al. (2024) with some modifications. The outer skin of the fruit was observed every two days and evaluated using a shrinkage index scale (1−10), where each index represented incremental ranges of 0–10 %, 10–20 %, 20–30 %, 30–40 %, 40–50 %, 50–60 %, 60–70 %, 70–80 %, 80–90 %, and 90–100 %, respectively.

2.7. Statistical analysis

Three independent replicates were performed for each group of samples to ensure statistical independence. The experimental data were analyzed by one-way ANOVA using SPSS 27.0 and Duncan's multiple ANOVA significant difference analysis tests Results were presented as mean ± standard deviation, with statistical significance defined as $p \leq 0.05$.

3. Results and discussions

3.1. Thickness, color and opacity of PE composite films

Generally, the incorporation of TP and GO resulted in thicker PE films. As depicted in Table 1, the thickness of the PE film was 65.40 ± 9.05 μm. The addition of both TP and GO resulted in varied increases in film thickness, with PE-GO showing the highest thickness. Interestingly, the PE-TP-GO film exhibited a slightly lower thickness of 71.19 ± 6.89 μm compared to PE-GO, possibly due to the good compatibility among the components resulting in a denser structure. Moreover, TP, a red powder, and GO, a black liquid, influenced the color of the PE film upon mixing. As illustrated in Figure 1A, the pure PE film appeared colorless and transparent. The addition of TP gave the film a light red hue while preserving its transparency. The incorporation of GO resulted in a tan-colored film, consistent with findings from prior research (Yang et al., 2020).

Similarly, Table 1 results indicate that incorporating 1 %GO (*w*/w) led to significant changes in the color metrics of the films, characterized by decreased L^* values and increased a^* and b^* values. Notably, PE-TP-GO films exhibited the lowest L^* values of 62.96 ± 2.83. Furthermore, the addition of GO contributed to increased opacity of the PE films; initially, the pure PE film had an opacity of 2.83 ± 0.11 %, which increased to 8.20 ± 0.30 % with the incorporation of TP and GO (Fig. 1B). Previous studies indicates that the incorporation of GO and TP diminishes the opacity of the composite film while improving its UV barrier properties, largely attributed to the UV-absorbing characteristics of GO and TP (Kafashan & Babaei, 2024; Lei et al., 2019).

These changes in film brightness and opacity help reduce oxidative and enzymatic damage to packaged foods caused by UV and visible light exposure, minimizing problems like discoloration, nutrient loss, and off-flavors (Rubilar et al., 2013).

Values with the same row in a column on the same day are not significantly different according to Duncan's Multiple Range Test ($P \leq 0.05$). The data are presented with standard errors of the means ($n \geq 3$).

3.2. FTIR, XRD and TGA analysis

FTIR is primarily utilized to analyze interactions among components and chemical groups in biopolymer-based food packaging films (Zhang & Jiang, 2020). The FTIR results are presented in Fig. 2. The broad absorption band spanning 3400 to 2500 cm^{-1} primarily arises from the stretching vibrations of intermolecular and intramolecular hydrogen bonds within PE. Upon the addition of TP, a slight reduction in intensity was observed in this broad peak region compared to the pure PE film. This decrease may be due to the formation of hydrogen bonds between TP and PE, thereby reducing the availability of free hydroxyl groups in PE. Other studies have reported similar findings, where the incorporation of apple polyphenols decreased the broadening of -OH bonds, suggesting the ability of polyphenols to engage in hydrogen bonding with polymer molecules (Nisar et al., 2019). The peak signals at 2936 cm^{-1} primarily correspond to the -CH stretching vibration. It was noted that the addition of both TP and GO resulted in a slight redshift of the absorption peak located at 2936 cm^{-1}. The bands at 1740 cm^{-1} and 1640 cm^{-1} correspond to the C═O and -COOH stretching vibrations, respectively (Shankar, Tanomrod, Rawdkuen, & Rhim, 2016). The peak at 1228 cm^{-1} is attributed to the C—O stretching of carboxylic acids (Viana, Sá, Barros, de Fátima Borges, & 2018). The peak at 1015 cm^{-1} corresponds to the C–O–C stretching vibrations of the polygalacturonic acid structure (Go & Song, 2020). The peak at 922 cm^{-1} corresponds to the absorption peak of α-D-mannopyranose (Younis & Zhao, 2019). Upon a comprehensive review of the FTIR spectra in this study, the incorporation of TP and GO into pure PE did not introduce new peaks nor induce significant alterations in existing peaks compared to pure PE films. This observation indicates that the addition of TP and GO does not alter the chemical structure of PE. Yang et al. (2020) also found that the cross-linking effect of GO addition on alginate films was primarily physical interactions, such as hydrogen bonding.

Additionally, XRD analysis was conducted in this study to evaluate how the incorporation of various polymers affects the crystal structure of PE composite films. Peaks associated with pure pectin have been reported at 12.7°, 16.72°, 18.42°, 21.5°, 25.32°, and 40.14° (2θ) (Meneguin, Cury, & Evangelista, 2014; Sartori et al., 2018). In this study, the peak of the pure PE film was observed at 17.6°, which is characteristic of the amorphous nature inherent to this biopolymer (Fig. 3). The distinct peaks related to crystallinity were observed in PE composite films containing TP and GO, with no significant shifts in peak positions, suggesting that TP and GO did not modify the amorphous structure of the PE films. However, the addition of TP and GO resulted in a decrease in curve intensity, which may be attributed to reduced intramolecular hydrogen bonding interactions within PE due to intermolecular hydrogen bonding interactions of TP and GO with PE, thereby decreasing the intermolecular attraction of PE. Similar findings have been reported in previous studies (Cabello, Takara, Marchese, & Ochoa, 2015; Nisar et al., 2019). In PE-GO films, the peak at 17.6° was observed to broaden, suggesting the effective integration of GO into the PE matrix, a phenomenon also noted by Panda et al. (2022). No new diffraction peaks were detected in any of the composite PE films.

The thermal analysis diagrams of TGA and DTG are presented in Fig. 4. The thermal decomposition profiles of both pure PE film and PE composite film in this study exhibit three distinct stages, consistent with previous findings (Shankar et al., 2016; Zhang et al., 2020). The initial weight loss stage, occurring at about 75 °C, is attributed to the evaporation of loosely bound water from the film. The second stage, between 170 and 220 °C, corresponds to glycerol and pectin polymers decomposition (Gorrasi, Bugatti, & Vittoria, 2012; Shankar & Rhim, 2015). The third stage occurred between 270 and 350 °C and corresponded to the oxidation zone, is primarily attributed to the oxidation of polymers, TP and GO (Fathi, Babaei, & Rostami, 2022). In the PE-TP-GO films, it was observed that the thermal decomposition residue in the initial stage was slightly higher compared to pure PE films. Furthermore, in the second stage of thermal decomposition, PE-TP-GO exhibited a higher maximum decomposition temperature than pure PE film, similar to observations in PE-TP films, suggesting enhanced thermal stability in PE-TP-GO films. The decomposition temperature of PE-TP-GO film is lower than that of PE-TP film, which may be due to the tpyrolysis of oxygen functional groups on the surface of GO (Pandele et al., 2017). Other studies have shown that cross-linking polyphenols, such as TP and apple peel polyphenols, can enhance the thermal stability of composite films (Lei et al., 2019; Maroufi, Shahabi, Ghanbarzadeh, & Ghorbani, 2022).

Table 1
Thickness, color and opacity of PE, PE-GO, PE-TP and PE-TP-GO films.

Films	PE	PE-GO	PE-TP	PE-TP-GO
Thickness (μm)	65.40 ± 9.05^{c}	75.04 ± 5.14^{a}	69.76 ± 4.65^{b}	71.19 ± 6.89^{b}
L^*	87.36 ± 0.48^{a}	67.15 ± 2.23^{c}	83.59 ± 0.35^{b}	62.96 ± 2.83^{d}
a^*	0.72 ± 0.12^{d}	2.39 ± 0.38^{b}	1.06 ± 0.04^{c}	3.02 ± 0.57^{a}
b^*	2.06 ± 0.95^{c}	21.92 ± 1.84^{a}	4.24 ± 0.50^{b}	21.82 ± 2.00^{a}
Opacity (A mm^{-1})	2.83 ± 0.11^{d}	6.69 ± 0.27^{b}	3.26 ± 0.08^{c}	8.20 ± 0.30^{a}

3.3. SEM of PE composite films

In this study, SEM was employed to analyze the surface and cross-sectional morphology of the PE composite films, facilitating a detailed observation of their microstructure. As depicted in Fig. 5, at 1000× magnification, all PE films exhibited overall uniform surfaces with no cracks, indicating the PE matrix's excellent film-forming properties and

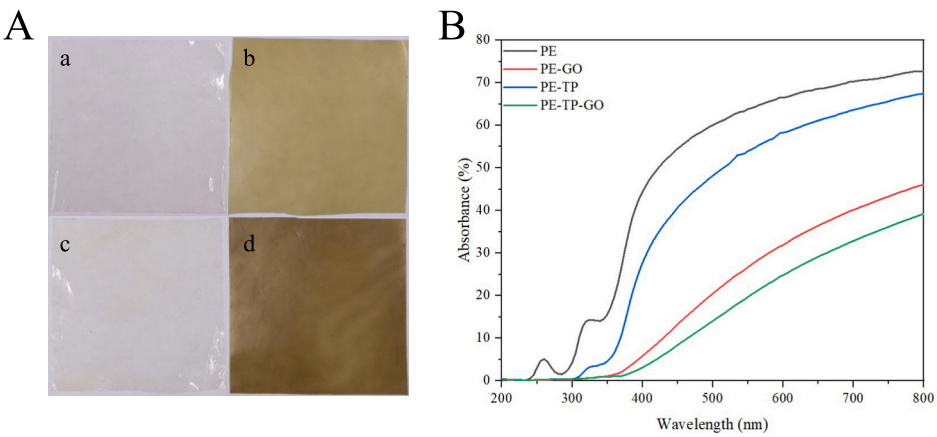

Fig. 1. Photographic schematic (a: PE b: PE-GO; c: PE-TP; d: PE-TP-GO) of PE composite film and UV absorption spectra of PE composite film.

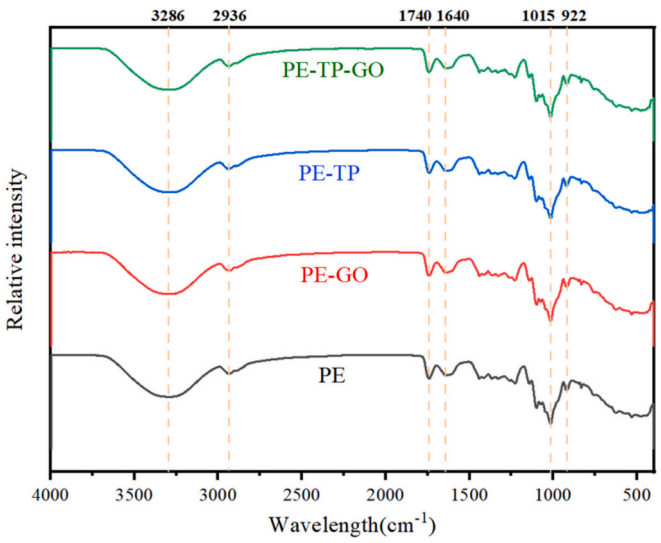

Fig. 2. FTIR spectra of PE, PE-GO, PE-TP and PE-TP-GO films.

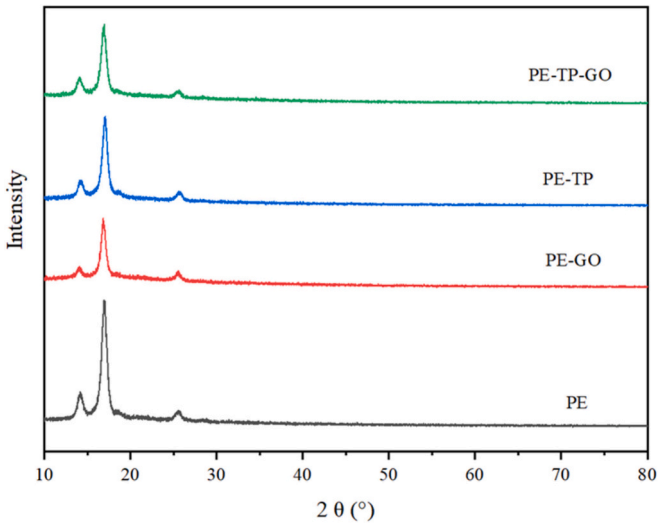

Fig. 3. X-crystal diffraction patterns of PE, PE-GO, PE-TP and PE-TP-GO films.

homogeneous dispersion of components within it. Fig. 5 also reveals that pure PE films exhibited surface pits absent in other groups, suggesting a significant reduction in porosity and showed a dense and continuous cross-section in the PE-TP-GO films. This phenomenon indicates that TP and GO interactions fill gaps between PE molecules, leading to a denser molecular arrangement and consequently influencing the mechanical strength of the PE composite films. Furthermore, the uneven small particle bumps on the GO-added film surfaces may be ascribed to aggregation events due to elevated GO concentrations, aligning with previous research (Ahmed, Mulla, & Arfat, 2017). The cross-section (Fig. 6) reveals a uniform and continuous structure of the PE composite film without voids or delamination, indicating good compatibility among pectin, TP and GO. Additionally, an increase in cross-sectional roughness was observed with the addition of GO, which may result from interactions between polymer chains and the oxygen functional groups of GO, consistent with findings by Alves, Ferreira, Ferreira, and Nunes (2022).

3.4. MC, WVP and WCA of PE composite films

The incorporation of both TP and GO into the pure PE film led to reductions in MC, WVP, and WCA of the composite film. Regarding MC (Table 2), the addition of TP and GO resulted in decreased film MC, with GO exerting a more pronounced effect. This may be due to the interaction of GO and TP with polysaccharide molecules through potential hydrogen bonding, thus limiting the interaction of PE chains with water molecules and decreasing the water absorption ability of the films. Similar trends were observed in citrus pectin films enriched with thinned young apple polyphenols and soluble soybean polysaccharide films with GO added (Kafashan, Joze-Majidi, Kazemi-Pasarvi, Babaei, & Jafari, 2023; Nisar et al., 2019). Among them, PE-TP-GO exhibited the lowest WCA of 52.44 ± 0.64°. Kafashan et al. (2023) similarly observed a decrease in MC when studying the addition of grape skin anthocyanins and GO to soluble soybean polysaccharide.

The WVP reflects the water barrier properties of the films. Analysis of the data in Table 2, the WVP of the composite film containing both TP and GO is significantly lower ($p \leq 0.05$) compared to the other films, decreasing from 1.30 ± 0.12 ($\times 10^{-10}$ $g^{-1}s^{-1}Pa^{-1}$) for the pure PE film to 0.67 ± 0.17 ($\times 10^{-10}$ $g^{-1}s^{-1}Pa^{-1}$). This reduction is likely due to the interaction of TP and GO with PE molecules via hydrogen bonding, which diminishes the film's affinity for water. Consequently, this interaction impedes the movement of water molecules through the film and decreases their diffusion rate (Zhang et al., 2020). Similar findings of reduced WVP were also noted in chitosan composite films enriched with green tea extract (Siripatrawan & Harte, 2010). Yang et al. (2020) also reported comparable outcomes when GO materials were incorporated into polymer matrices.

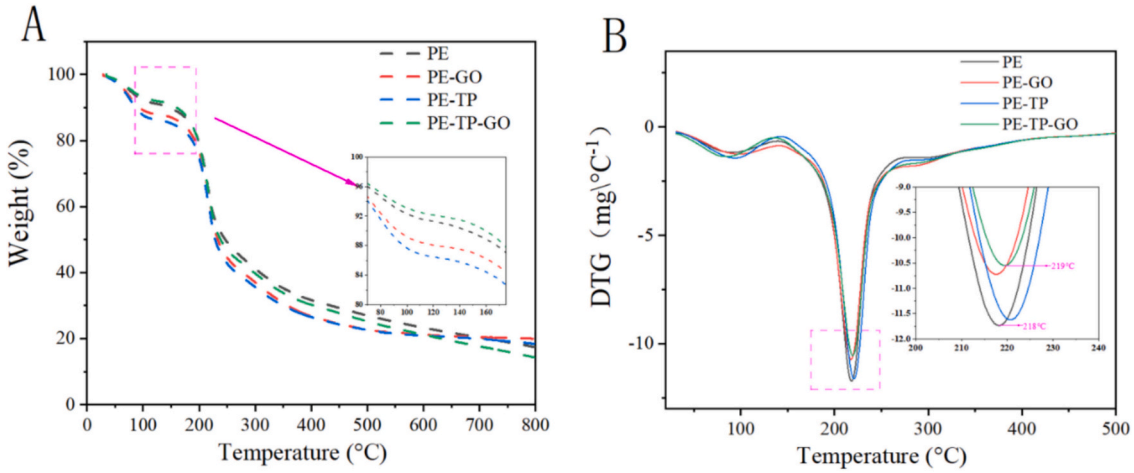

Fig. 4. TGA of PE, PE-GO, PE-TP and PE-TP-GO films.

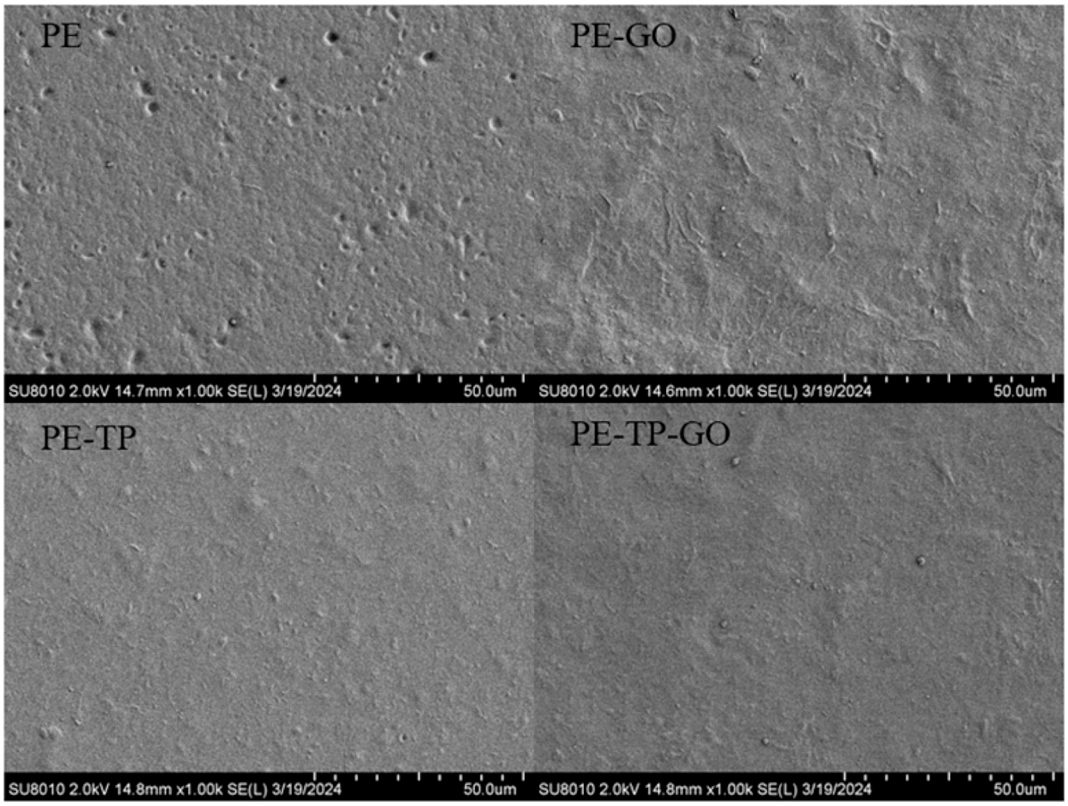

Fig. 5. SEM electron micrographs of the surface of PE, PE-GO, PE-TP and PE-TP-GO films.

The WCA reflects the material's hydrophilic and hydrophobic properties, offering insights into the surface wettability of the film. Data from Table 2 reveal that PE films containing TP exhibit reduced hydrophilicity, as evidenced by an increase in the WCA of PE-TP films from 61.90° to 79.80° compared to PE film. This increase may result from interactions between TP and the hydroxyl groups on the PE molecular chain, which reduce the exposure of hydroxyl groups on the film surface and consequently decrease its hydrophilicity. After the addition of WI-TPN, the WVP of the PE WI-TPN composite membrane also showed a similar trend (Yang et al., 2024). Conversely, the decrease in WCA observed in PE-TP-GO films is due to electrostatic and hydrogen bonding interactions between PE and the oxygen-containing groups of GO, which lead to an increased exposure of hydroxyl groups on the film surface. Furthermore, the incorporation of GO enhances the surface roughness of the composite films. These effects collectively contribute to the WCA of PE-TP-GO films is approximately 8.33° lower than that of PE-TP films. Similar observations were reported in a study where reduced GO (rGO) was incorporated into a chitosan matrix, showing the decrease in WCA may be attributed to both the residual oxygen-containing groups of rGO and the impact of rGO on the surface roughness of the material (Barra et al., 2019).

Values with the same letter in a column on the same day are not significantly different according to Duncan's Multiple Range Test ($P \leq 0.05$). The data are presented with standard errors of the means ($n \geq 3$).

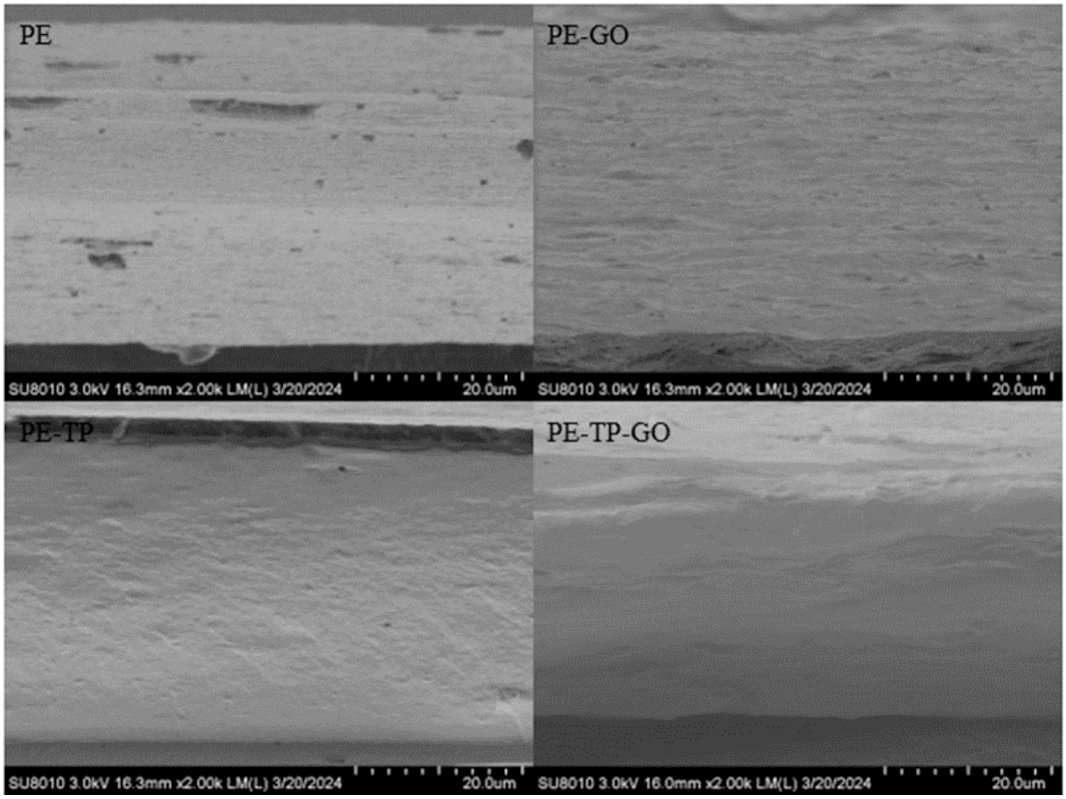

Fig. 6. Cross-sectional SEM electron micrographs of PE, PE-GO, PE-TP and PE-TP-GO films.

Table 2
MC, WVP, WCA and Young's Modulus of PE, PE-GO, PE-TP and PE-TP-GO films.

Films	MC (%)	WVP ($\times 10^{-10}$ $g^{-1}s^{-1}Pa^{-1}$)	WCA (°)	Young's Modulus (MPa)
PE	72.67 ± 1.86^{a}	1.30 ± 0.12^{a}	61.90 ± 0.33^{d}	63.36 ± 1.40^{b}
PE-GO	53.43 ± 1.03^{c}	1.04 ± 0.24^{a}	62.82 ± 0.73^{c}	80.59 ± 1.89^{a}
PE-TP	59.38 ± 1.35^{b}	1.15 ± 0.19^{a}	79.80 ± 0.66^{a}	47.98 ± 1.06^{d}
PE-TP-GO	52.44 ± 0.64^{c}	0.67 ± 0.17^{b}	71.47 ± 0.19^{b}	60.17 ± 1.08^{c}

3.5. Mechanical properties

Food packaging materials must exhibit specific mechanical properties for practical applications, particularly in transportation and preservation, which are crucial for maintaining product integrity (Mir, Dar, Wani, & Shah, 2018). Therefore, this study evaluated the TS and EB of the films (Fig. 7) to assess their mechanical performance. Fig. 7A presents the TS and EB variations of both pure PE films and PE composite films, while Fig. 7B illustrates the corresponding stress-strain relationships. The results indicated that pure PE films exhibited the lowest TS (17.13 MPa) and EB (24.53 %). Incorporating GO significantly increased the TS values of the films, with the PE-GO film having the highest TS

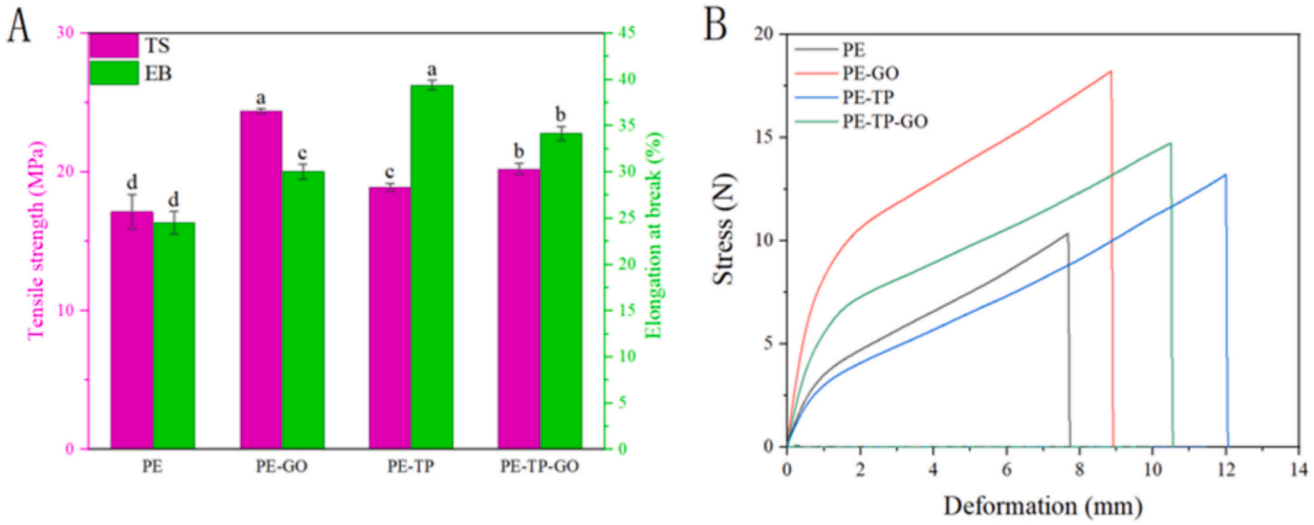

Fig. 7. Schematic representation of mechanical properties and stress profile of PE, PE-GO, PE-TP and PE-TP-GO films.

value and Young's modulus of about 24.40 MPa and 80.59 MPa, respectively. This enhancement in TS results from favorable interfacial interactions between GO and the PE matrices. A related study investigating the impact of the non-covalent functionality of GO on the mechanical properties of PE composite films reported similar findings (Pandele et al., 2017). It is noteworthy that an optimal concentration of GO positively enhances the mechanical properties of the composite film. However, at excessively high concentrations, GO tends to aggregate rather than disperse uniformly within the film structure, resulting in reduced mechanical properties. This aspect has been verified through preliminary experiments to determine the appropriate addition concentration. Furthermore, the addition of TP significantly enhances the EB of the films, exemplified by the superior EB value of PE-TP films (39.38 %). However, the Young's modulus of the PE-TP film decreased to 47.98 MPa similar improvement in the mechanical properties of PE-chitosan films was noted upon TP addition. This enhancement can be attributed to the chemical composition of TP, which contains numerous hydrophilic groups capable of forming extensive hydrogen bonds with the substrate, thereby imparting favorable physical properties to the films (Gao et al., 2019). Consequently, incorporating both 1 % (*w*/w) GO and 1 % (w/w) TP has the potential to enhance the mechanical performance of PE films. The resulting PE-TP-GO films demonstrated exceptional mechanical properties with a TS of 20.22 MPa and EB of 34.18 %.

3.6. Antioxidant activity

As depicted in Fig. 8, the pure PE film showed low antioxidant activity, with DPPH radical scavenging and ABTS radical scavenging rates of 42.11 % and 14.53 %, respectively. Interestingly, incorporating GO did not enhance the antioxidant activity of the films; instead, it led to a slight decrease of 3.51 % in the ABTS radical scavenging rate and an increase of 14.63 % in the DPPH radical scavenging rate. The addition of GO did not exhibit a significant antioxidant effect, primarily because GO is a poor H-donor antioxidant (Qiu et al., 2014). PE-TP films exhibited the highest ABTS radical scavenging rate, with DPPH radical scavenging rate and ABTS radical scavenging rate reaching 71.62 % and 96.45 %, respectively. The addition of TP and GO also significantly enhanced the antioxidant activity of the PE-TP-GO composite films, with the DPPH radical scavenging rate reaching a maximum of 80.41 % and a remarkable 75.94 % increase in ABTS radical scavenging rate compared to the pure PE film. These improvements can be due to the redox properties inherent to phenolic compounds. These results align with previous studies showing that TP significantly boosts the antioxidant properties of PE films (Lei et al., 2019; Nisar et al., 2019).

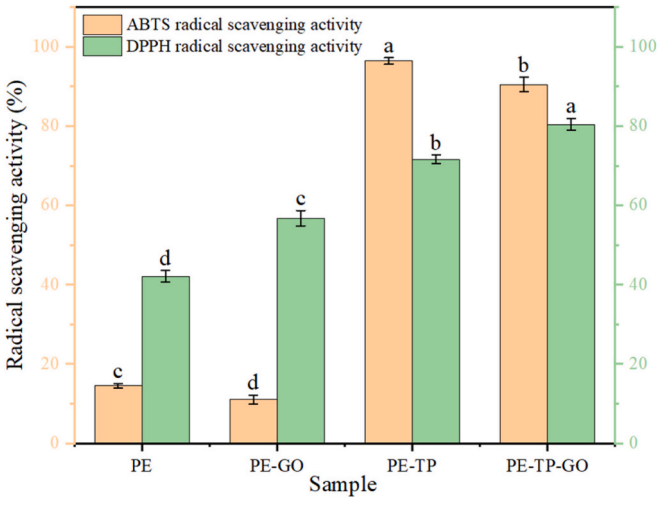

Fig. 8. Free radical scavenging rate and total antioxidant capacity of PE, PE-GO, PE-TP and PE-TP-GO films.

3.7. TP release property

In this study, we examined the slow-release characteristics of TP from PE films incorporating GO to demonstrate that GO has the capability to facilitate gradual substance release. Fig. 9 illustrates that the release profile of the films can be categorized into two distinct stages. Initially, within the first 12 h, both PE-TP films and PE-TP-GO films exhibited a rapid release of TP, possibly attributed to residual TP on the film surface. Subsequently, TP was released slowly release during the second phase. Similar release patterns of active substances were observed in chitosan-based films supplemented with curcumin (Ni et al., 2022). Additionally, the results indicated that the PE-TP-GO films demonstrated better slow-release performance compared to the pure PE films. By the fourth day, the release of TP from the control group declined, while the release from the PE-TP-GO film increased. This may be due to reduced TP loading in the film resulting from the excessive release of TP in the control group, which consequently impacted the antioxidant activity of the film. These findings suggest that PE-TP-GO films containing GO can significantly control the release of TP. This effect may be attributed to the abundant oxygen-containing functional groups on the surface of GO, which interact with PE to form a dense PE-GO network, thereby reducing the release of loaded TP. Similarly, GO exhibited a controlled release effect for anthocyanins (Fathi et al., 2022; Kafashan et al., 2023; Kafashan & Babaei, 2024).

3.8. Application of PE composite films in blueberry fruits packaging

During storage, transpiration and respiration processes in blueberries can lead to both cosmetic crumpling and weight loss (Liu, Xue, Li, & Adhikari, 2022). Fig. 10A illustrates a consistent weight loss across all blueberries during storage. Notably, control samples experienced significant weight reduction compared to film-packed samples due to the direct exposure of the control samples to the external environment. The film-packed treatment group exhibited reduced weight loss owing to the film barrier properties. The PE-TP-GO film demonstrated the least weight loss, aligning with results from WVP tests. The PE-TP-GO film, characterized by its minimal WVP, effectively limits water loss from fruits and vegetables during storage, thereby preserving their quality. Freshness assessment can also be directly inferred from the visual appearance of blueberries, as depicted in Fig. 10C illustrating changes over an 8-day storage period. Initially, all blueberries exhibited a smooth and plump appearance. By the end of the storage period, the control group displayed noticeable wrinkling and the presence of mold mycelium. In contrast, the fruits in the film-packed group maintained a significantly better appearance. Particularly, blueberries packed in PE-TP-GO film exhibited the highest visual quality, showing minimal change compared to their initial appearance. Thus, the use of PE-TP-GO film effectively mitigates water loss in fruits and vegetables during storage, preserving their complete appearance and overall quality, thereby enhancing their commercial value (Feng, Fan, He, & Ma, 2024).

4. Conclusions

In summary, PE-based polysaccharide films with synergistic reinforcement of TP and GO were successfully prepared in this study. The addition of TP (1 % *w*/w) and GO (1 % w/w) enhanced the physical and mechanical properties of pure PE films. Specifically, the TS and EB of PE-TP-GO films increased by approximately 3.09 MPa and 9.65 %, respectively, compared to pure PE films. The incorporation of GO significantly improved the barrier properties of the PE films, including WVP ($0.67 \pm 0.17 \times 10^{-10} \times 10^{-10}$ $g^{-1}s^{-1}Pa^{-1}$) and light opacity (8.20 $\pm$ 0.30 A mm^{-1}). Additionally, GO enhanced the stability of TP, prolonging its active release. The composite films showed a homogeneous appearance, indicating good compatibility between the components. This compatibility was also evident in the microstructure of the composite film, which displayed a smooth surface and a continuous, dense

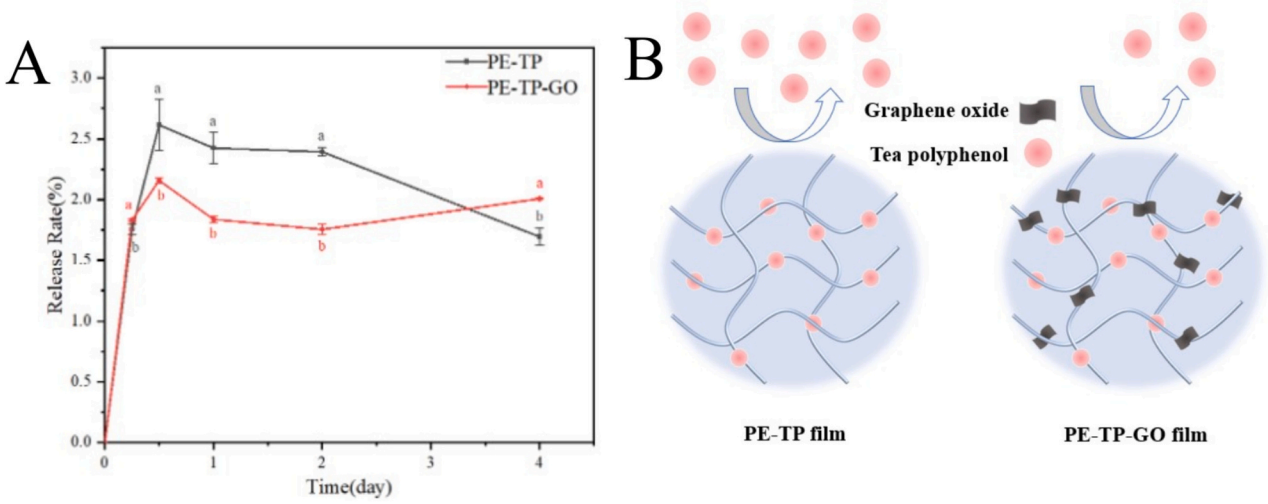

Fig. 9. Release rate (A) and release mechanism (B) of TP from PE-TP and PE-TP-GO films.

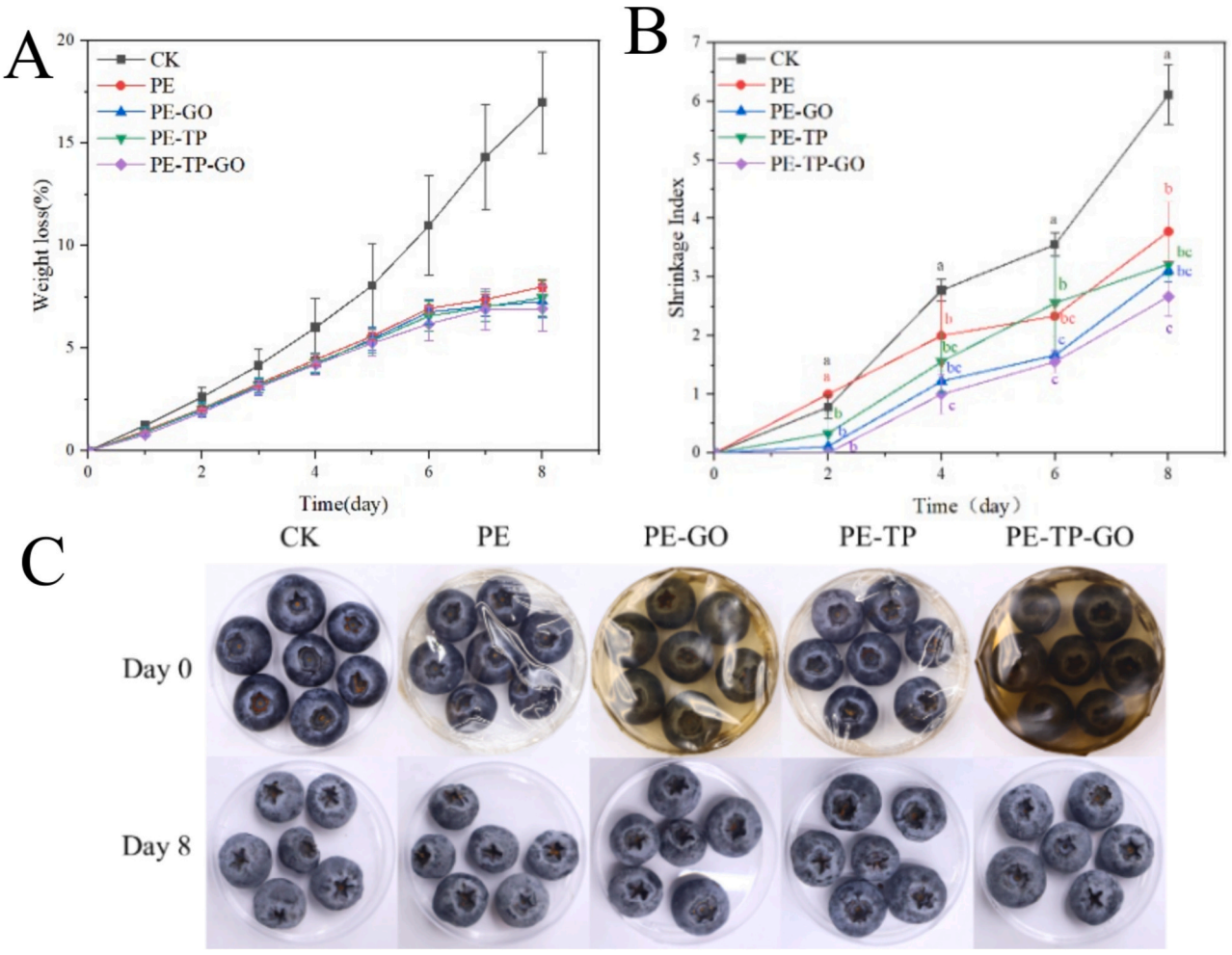

Fig. 10. Weight loss (A), shrinkage index (B) and photographs of the appearance (C) of untreated and PE composite coating-treated blueberries over 8 days. CK refers to the blank control group.

cross-section in the PE-TP-GO film. In blueberry fruits preservation tests, fruits packaged in PE-TP-GO films showed the lowest weight loss and shrinkage index, maintaining a better appearance after eight days of storage. The presence of GO diminished the visibility of the fruit, potentially influencing consumers' evaluations of packaged foods. Additionally, the application of PE-TP-GO film packaging in diverse fruits and vegetables requires more investigation.

CRediT authorship contribution statement

Zixuan Li: Writing – original draft, Visualization, Methodology, Investigation, Formal analysis, Data curation, Conceptualization. **Mohammad Rizwan Khan:** Writing – review & editing, Funding acquisition, Formal analysis. **Naushad Ahmad:** Writing – review & editing, Funding acquisition, Formal analysis. **Wanli Zhang:** Writing – review & editing, Writing – original draft, Validation, Supervision, Software, Methodology, Funding acquisition, Formal analysis, Data curation, Conceptualization. **Gulden Goksen:** Writing – review & editing, Visualization, Validation, Formal analysis, Data curation, Conceptualization.

Acknowledgements

This work was supported by Hainan Provincial Natural Science Foundation of China (324RC460). The authors would also like to thank the Researchers Supporting Project Number (RSP2025R138), King Saud University, Riyadh, Saudi Arabia.

Data availability

Data will be made available on request.

References

Ahmed, J., Mulla, M., & Arfat, Y. A. (2017). Mechanical, thermal, structural and barrier properties of crab shell chitosan/graphene oxide composite films. *Food Hydrocolloids, 71*, 141–148.

Alves, Z., Ferreira, N. M., Ferreira, P., & Nunes, C. (2022). Design of heat sealable starch-chitosan bioplastics reinforced with reduced graphene oxide for active food packaging. *Carbohydrate Polymers, 291*, Article 119517.

Barra, A., Ferreira, N. M., Martins, M. A., Lazar, O., Pantazi, A., Jderu, A. A., & Nunes, C. (2019). Eco-friendly preparation of electrically conductive chitosan-reduced graphene oxide flexible bionanocomposites for food packaging and biological applications. *Composites Science and Technology, 173*, 53–60.

Cabello, S. P., Takara, E. A., Marchese, J., & Ochoa, N. A. (2015). Influence of plasticizers in pectin films: Microstructural changes. *Materials Chemistry and Physics, 162*, 491–497.

Chen, F., & Chi, C. (2021). Development of pullulan/carboxylated cellulose nanocrystal/tea polyphenol bionanocomposite films for active food packaging. *International Journal of Biological Macromolecules, 186*, 405–413.

Fathi, M., Babaei, A., & Rostami, H. (2022). Development and characterization of locust bean gum-Viola anthocyanin-graphene oxide ternary nanocomposite as an efficient pH indicator for food packaging application. *Food Packaging and Shelf Life, 34*, Article 100934.

Feng, Q., Fan, B., He, Y. C., & Ma, C. (2024). Antibacterial, antioxidant and fruit packaging ability of biochar-based silver nanoparticles-polyvinyl alcohol-chitosan composite film. *International Journal of Biological Macromolecules, 256*, Article 128297.

Gao, H. X., He, Z., Sun, Q., He, Q., & Zeng, W. C. (2019). A functional polysaccharide film formed by pectin, chitosan, and tea polyphenols. *Carbohydrate Polymers, 215*, 1–7.

Go, E. J., & Song, K. B. (2020). Development and characterization of citrus junos pomace pectin films incorporated with rambutan (Nephelium lappaceum) peel extract. *Coatings, 10*(8), 714.

Gorrasi, G., Bugatti, V., & Vittoria, V. (2012). Pectins filled with LDH-antimicrobial molecules: Preparation, characterization and physical properties. *Carbohydrate Polymers, 89*(1), 132–137.

Guo, Y., Duan, B., Cui, L., & Zhu, P. (2015). Construction of chitin/graphene oxide hybrid hydrogels. *Cellulose, 22*, 2035–2043.

He, J., Yang, S., Goksen, G., Cong, X., Khan, M. R., & Zhang, W. (2024). Functionalized pectin/alginate food packaging films based on metal-phenol networks. *Food Bioscience, 58*, Article 103635.

Kafashan, A., & Babaei, A. (2024). Development and investigation of a polysaccharide ternary nanocomposite based on basil seed gum/graphene oxide/anthocyanin for intelligent food packaging. *International Journal of Biological Macromolecules, 280*, Article 135537.

Kafashan, A., Joze-Majidi, H., Kazemi-Pasarvi, S., Babaei, A., & Jafari, S. M. (2023). Nanocomposites of soluble soybean polysaccharides with grape skin anthocyanins and graphene oxide as an efficient halochromic smart packaging. *Sustainable Materials and Technologies, 38*, Article e00755.

Lee, D. W., De Los, S. V., & L., Seo, J. W., Felix, L. L., Bustamante D, A., Cole, J. M., & Barnes, C. H. W.. (2010). The structure of graphite oxide: Investigation of its surface chemical groups. *The Journal of Physical Chemistry B, 114*(17), 5723–5728.

Lei, Y., Wu, H., Jiao, C., Jiang, Y., Liu, R., Xiao, D., & Li, S. (2019). Investigation of the structural and physical properties, antioxidant and antimicrobial activity of pectin-konjac glucomannan composite edible films incorporated with tea polyphenol. *Food Hydrocolloids, 94*, 128–135.

Liu, D., Bian, Q., Li, Y., Wang, Y., Xiang, A., & Tian, H. (2016). Effect of oxidation degrees of graphene oxide on the structure and properties of poly (vinyl alcohol) composite films. *Composites Science and Technology, 129*, 146–152.

Liu, X., Xue, F., Li, C., & Adhikari, B. (2022). Physicochemical properties of films produced using nanoemulsions stabilized by carboxymethyl chitosan-peptide conjugates and application in blueberry preservation. *International Journal of Biological Macromolecules, 202*, 26–36.

Maroufi, L. Y., Shahabi, N., Ghanbarzadeh, M. D., & Ghorbani, M. (2022). Development of antimicrobial active food packaging film based on gelatin/dialdehyde quince seed gum incorporated with apple peel polyphenols. *Food and Bioprocess Technology, 15*(3), 693–705.

Meneguin, A. B., Cury, B. S. F., & Evangelista, R. C. (2014). Films from resistant starch-pectin dispersions intended for colonic drug delivery. *Carbohydrate Polymers, 99*, 140–149.

Miao, Z., Zhang, Y., & Lu, P. (2021). Novel active starch films incorporating tea polyphenols-loaded porous starch as food packaging materials. *International Journal of Biological Macromolecules, 192*, 1123–1133.

Mir, S. A., Dar, B. N., Wani, A. A., & Shah, M. A. (2018). Effect of plant extracts on the techno-functional properties of biodegradable packaging films. *Trends in Food Science & Technology, 80*, 141–154.

Mohnen, D. (2008). Pectin structure and biosynthesis. *Current Opinion in Plant Biology, 11*(3), 266–277.

Nesic, A., Meseldzija, S., Cabrera-Barjas, G., & Onjia, A. (2022). Novel biocomposite films based on high methoxyl pectin reinforced with zeolite Y for food packaging applications. *Foods, 11*(3), 360.

Ni, Y., Nie, H., Wang, J., Lin, J., Wang, Q., Sun, J., & Wang, J. (2022). Enhanced functional properties of chitosan films incorporated with curcumin-loaded hollow graphitic carbon nitride nanoparticles for bananas preservation. *Food Chemistry, 366*, Article 130539.

Nisar, T., Wang, Z. C., Alim, A., Iqbal, M., Yang, X., Sun, L., & Guo, Y. (2019). Citrus pectin films enriched with thinned young apple polyphenols for potential use as bio-based active packaging. *CyTA-Journal of Food, 17*(1), 695–705.

Panda, P. K., Dash, P., Yang, J. M., & Chang, Y. H. (2022). Development of chitosan, graphene oxide, and cerium oxide composite blended films: Structural, physical, and functional properties. *Cellulose*, 1–13.

Pandele, A. M., Andronescu, C., Vasile, E., Radu, I. C., Stanescu, P., & Iovu, H. (2017). Non-covalent functionalization of GO for improved mechanical performances of pectin composite films. *Composites Part A: Applied Science and Manufacturing, 103*, 188–195.

Qiu, Y., Wang, Z., Owens, A. C., Kulaots, I., Chen, Y., Kane, A. B., & Hurt, R. H. (2014). Antioxidant chemistry of graphene-based materials and its role in oxidation protection technology. *Nanoscale, 6*(20), 11744–11755.

Rubilar, J. F., Cruz, R. M., Silva, H. D., Vicente, A. A., Khmelinskii, I., & Vieira, M. C. (2013). Physico-mechanical properties of chitosan films with carvacrol and grape seed extract. *Journal of Food Engineering, 115*(4), 466–474.

Sadadekar, A. S., Shruthy, R., Preetha, R., Kumar, N., Pande, K. R., & Nagamaniammai, G. (2023). Enhanced antimicrobial and antioxidant properties of Nano chitosan and pectin based biodegradable active packaging films incorporated with fennel (Foeniculum vulgare) essential oil and potato (Solanum tuberosum) peel extracts. *Journal of Food Science and Technology, 60*(3), 938–946.

Sartori, T., Feltre, G., & do Amaral Sobral, P. J., da Cunha, R. L., & Menegalli, F. C.. (2018). Properties of films produced from blends of pectin and gluten. *Food Packaging and Shelf Life, 18*, 221–229.

Senanayake, S. N. (2013). Green tea extract: Chemistry, antioxidant properties and food applications–A review. *Journal of Functional Foods, 5*(4), 1529–1541.

Shankar, S., & Rhim, J. W. (2015). Amino acid mediated synthesis of silver nanoparticles and preparation of antimicrobial agar/silver nanoparticles composite films. *Carbohydrate Polymers, 130*, 353–363.

Shankar, S., Tanomrod, N., Rawdkuen, S., & Rhim, J. W. (2016). Preparation of pectin/silver nanoparticles composite films with UV-light barrier and properties. *International Journal of Biological Macromolecules, 92*, 842–849.

Siripatrawan, U., & Harte, B. R. (2010). Physical properties and antioxidant activity of an active film from chitosan incorporated with green tea extract. *Food Hydrocolloids, 24*(8), 770–775.

Viana, R. M., Sá, N. M., Barros, M. O., de Fátima Borges, M., & Azeredo, H. M. (2018). Nanofibrillated bacterial cellulose and pectin edible films added with fruit purees. *Carbohydrate Polymers, 196*, 27–32.

Yang, J., Cai, W., Rizwan Khan, M., Ahmad, N., Zhang, Z., Meng, L., & Zhang, W. (2023). Application of tannic acid and Fe3+ crosslinking-enhanced pectin films for passion fruit preservation. *Foods, 12*(18), 3336.

Yang, L., Yang, J., Qin, X., Kan, J., Zeng, F., & Zhong, J. (2020a). Ternary composite films with simultaneously enhanced strength and ductility: Effects of sodium alginate-gelatin weight ratio and graphene oxide content. *International Journal of Biological Macromolecules, 156*, 494–503.

Yang, L., Yang, J., Qin, X., Kan, J., Zeng, F., & Zhong, J. (2020b). Ternary composite films with simultaneously enhanced strength and ductility: Effects of sodium alginate-gelatin weight ratio and graphene oxide content. *International Journal of Biological Macromolecules, 156*, 494–503.

Yang, W., Zhang, S., Feng, A., Li, Y., Wu, P., Li, H., & Ai, S. (2024). Water-insoluble tea polyphenol nanoparticles as fillers and bioactive agents for pectin films to prepare active packaging for fruit preservation. *Food Hydrocolloids, 110364*.

Yang, Y., Shi, Y., Cao, X., Liu, Q., Wang, H., & Kong, B. (2021). Preparation and functional properties of poly (vinyl alcohol)/ethyl cellulose/tea polyphenol electrospun nanofibrous films for active packaging material. *Food Control, 130*, Article 108331.

Yoo, B. M., Shin, H. J., Yoon, H. W., & Park, H. B. (2014). Graphene and graphene oxide and their uses in barrier polymers. *Journal of Applied Polymer Science, 131*(1).
Younis, H. G., & Zhao, G. (2019). Physicochemical properties of the edible films from the blends of high methoxyl apple pectin and chitosan. *International Journal of Biological Macromolecules, 131*, 1057–1066.
Zhang, W., Cao, J., & Jiang, W. (2022). Effect of different cation in situ cross-linking on the properties of pectin-thymol active film. *Food Hydrocolloids, 128*, Article 107594.
Zhang, W., & Jiang, W. (2020). Antioxidant and antibacterial chitosan film with tea polyphenols-mediated green synthesis silver nanoparticle via a novel one-pot method. *International Journal of Biological Macromolecules, 155*, 1252–1261.
Zhang, W., Li, X., & Jiang, W. (2020). Development of antioxidant chitosan film with banana peels extract and its application as coating in maintaining the storage quality of apple. *International Journal of Biological Macromolecules, 154*, 1205–1214.
Zhang, W., Zhang, Y., Cao, J., & Jiang, W. (2021). Improving the performance of edible food packaging films by using nanocellulose as an additive. *International Journal of Biological Macromolecules, 166*, 288–296.
Zuo, P. P., Feng, H. F., Xu, Z. Z., Zhang, L. F., Zhang, Y. L., Xia, W., & Zhang, W. Q. (2013). Fabrication of biocompatible and mechanically reinforced graphene oxide-chitosan nanocomposite films. *Chemistry Central Journal, 7*, 1–11.